Computers and Mathematics with Applications 61 (2011) 1957–1962

Contents lists available at ScienceDirect

Computers and Mathematics with Applications

journal homepage: www.elsevier.com/locate/camwa

Application of the differential transformation method to bifurcation and chaotic analysis of an AFM probe tip

Cheng-Chi Wang [a,*], Her-Terng Yau [b]

[a] Department of Mechanical Engineering, Far East University, Hsin-Shih, Tainan, Taiwan

[b] Department of Electrical Engineering, National Chin-Yi University of Technology, Taichung, Taiwan

ARTICLE INFO

Keywords:
Bifurcation
Atomic force microscope
Differential transformation

ABSTRACT

The AFM (atomic force microscope) has become a popular and useful instrument for measuring intermolecular forces with atomic resolution, that can be applied in electronics, biological analysis, and studying materials, semiconductors etc. This paper conducts a systematic investigation into the bifurcation and chaotic behavior of the probe tip of an AFM using the differential transformation (DT) method. The validity of the analytical method is confirmed by comparing the DT solutions for the displacement and velocity of the probe tip at various values of the vibrational amplitude with those obtained using the Runge–Kutta (RK) method. The behavior of the probe tip is then characterized utilizing bifurcation diagrams, phase portraits, power spectra, Poincaré maps, and maximum Lyapunov exponent plots. The results indicate that the probe tip behavior is significantly dependent on the magnitude of the vibrational amplitude. Specifically, the tip motion changes first from subharmonic to chaotic motion, then from chaotic to multi-periodic motion, and finally from multi-periodic motion to subharmonic motion with windows of chaotic behavior as the non-dimensional vibrational amplitude is increased from 1.0 to 5.0.

1. Introduction

Recently, many significant researches have been carried out to design, analyze, and implement microsystems and nanosystems. The AFM enables the measurement of intermolecular forces at the atomic scale and is used extensively for imaging and measuring applications in the nanoelectronics, biological analysis, materials science, and semiconductors fields. Compared to the STM (scanning tunnel microscope), which is applicable only for conducting or semiconducting surfaces, the AFM can image virtually any type of surface, including glass, biological samples, polymers, ceramics, and so forth [1].

Analyzing the dynamic behavior of the AFM probe tip as it scans the surface of interest is a fundamental concern since any irregular motion during the scanning process inevitably degrades the precision of the measurement results. Consequently, the dynamic properties of the AFM tip–sample interaction have attracted extensive attention in the literature in recent years. Burnham et al. [2] showed experimentally that an AFM microcantilever performed chaotic motion under certain physical conditions. Ashhab et al. [3,4] analyzed the chaotic dynamics of the AFM cantilever–sample system using the Melnikov method and a single-frequency mode approximation. Sebastian et al. [5] predicted the dynamic behavior of an AFM cantilever in a tapping mode operation using a harmonic balancing and averaging technique. Lee et al. [6] analyzed the effects of van der Waals and Derjaguin–Muller–Toporov forces on the tip–sample interactions in dynamic force microscopy (DFM). Ruetzel et al. [7] applied the Galerkin method to investigate the nonlinear dynamics of an AFM probe tip under the assumption that the tip–surface interactions were governed by Lennard-Jones potentials.

* Corresponding author. Fax: +886 6 5979566x7211.
E-mail address: wccpipn@yahoo.com.tw (C.-C. Wang).

0898-1221/$ – see front matter © 2010 Elsevier Ltd. All rights reserved.
doi:10.1016/j.camwa.2010.08.019

The present study performs a systematic investigation into the dynamic behavior of an AFM probe tip using the DT method [8]. The validity of the analytical approach is confirmed by comparing the DT-based solutions for the displacement and velocity of the probe tip at various values of the vibrational amplitude with those obtained using the Runge–Kutta method. The dynamic response of the probe tip is then characterized using phase portraits, power spectra, Poincaré maps, and maximum Lyapunov exponent plots constructed using the time-series data obtained from the DT method. Finally, the onset of chaotic behavior in the AFM system is identified using bifurcation diagrams of the tip displacement and tip velocity, respectively.

2. The mathematical model of the cantilever tip–sample interaction

In the analysis performed in this study, the cantilever tip is modeled as a single spring–mass system comprising a sphere of radius R_s and an equivalent mass m_s suspended by a spring of stiffness k_s. The potential of the tip–sample assembly is given by [4]

$$P(X, Z) = -\frac{H_c R_S}{6\,(Z_b + X)} + \frac{1}{2} k_s X^2, \tag{1}$$

where Z_b is the equilibrium position of the tip, X is the tip displacement, $H_c = 2\pi\rho_1\rho_2 I_c$ is the Hamaker constant, and I_c is the interaction constant. In other words, the potential is modeled as the attraction force between a tip of radius R_s and density ρ_1 and a sample of density ρ_2.

The net energy of the system scaled by the mass m_s of the cantilever is given by

$$E(X, \dot{X}, Z) = \frac{1}{2}\dot{X}^2 + \frac{1}{2}\omega_s^2 X^2 - \frac{\xi\omega_s^2}{(Z_b + X)}, \tag{2}$$

where $\omega_s = \sqrt{k_s/m_s}$ is the first modal frequency of the system and $\xi = H_c R_s/6k_s$. Let $X_1 = X$ and $X_2 = \dot{X}$. The dynamics of the tip–sample system, i.e. $\dot{X}_1 = \partial E/\partial X_2$ and $\dot{X}_2 = -(\partial E/\partial X_1)$, can be expressed as

$$\dot{X}_1 = X_2, \tag{3}$$

$$\dot{X}_2 = -\omega_s^2 X_1 - \frac{\xi\omega_s^2}{(Z_b + X_1)^2}. \tag{4}$$

In general, the cantilever beam of an AFM is forced by a small sinusoidal signal $mf\cos\omega t$, where ω takes values around the natural frequency ω_s of the system. Furthermore, in most AFMs, the motion of the cantilever beam is damped by the surrounding air. Thus, the differential equations of the AFM system can be written as

$$\dot{X}_1 = X_2, \tag{5}$$

$$\dot{X}_2 = -\omega_s^2 X_1 - \frac{\xi\omega_s^2}{(Z_b + X_1)^2} - f\cos\phi - \mu X_2, \tag{6}$$

where μX_2 is the damping force per unit mass.

Introducing parameters $Y_1 = \frac{X_1}{Y_s}$, $Y_2 = \frac{X_2}{\omega_s Y_s}$, $Z = \frac{Z_b}{Y_s}$, $A_1 = \frac{4}{27}$, $A_2 = 1.2$, $A_3 = 1$, $A_4 = -2.9$, $A_5 = 0.1$, and $\Omega = \frac{\omega}{\omega_s}$, the system equations can be rewritten in non-dimensional form as

$$Y_1 = Y_2, \tag{7}$$

$$Y_2' = -A_1 Y_1 - \frac{A_1 A_2}{(Z + Y_1)^2} + A_3(A_4\cos\phi - A_5 Y_2), \tag{8}$$

with initial conditions of $Y_1 = 0$, and $Y_2 = 0$. Y_1 is the displacement of the probe tip (where a positive value indicates a displacement toward the sample), Y_2 is the velocity of the probe tip, and Z is the vibrational amplitude of the dither piezoelectric actuator which drives the tip. Note that both Y_1 and Z are non-dimensionalized by the gap between the tip and the sample under equilibrium conditions.

In solving Eqs. (7) and (8) using the DT method, the AFM system model is transformed with respect to the time domain, and thus the two equations become

$$\frac{k+1}{H}\bar{Y}_1(k+1) = \bar{Y}_2(k), \tag{9}$$

$$\text{and}\quad \frac{k+1}{H}\bar{Y}_2(k+1) = -A_1\bar{Y}_1(k) - \frac{A_1 A_2}{\left(Z + \bar{Y}_1(k)\right)^2} + A_3\left(A_4\Omega\frac{(\Omega H)^k}{k!}\cos\left(\frac{\pi k}{2}\right) - A_5\bar{Y}_2(k)\right), \tag{10}$$

respectively.

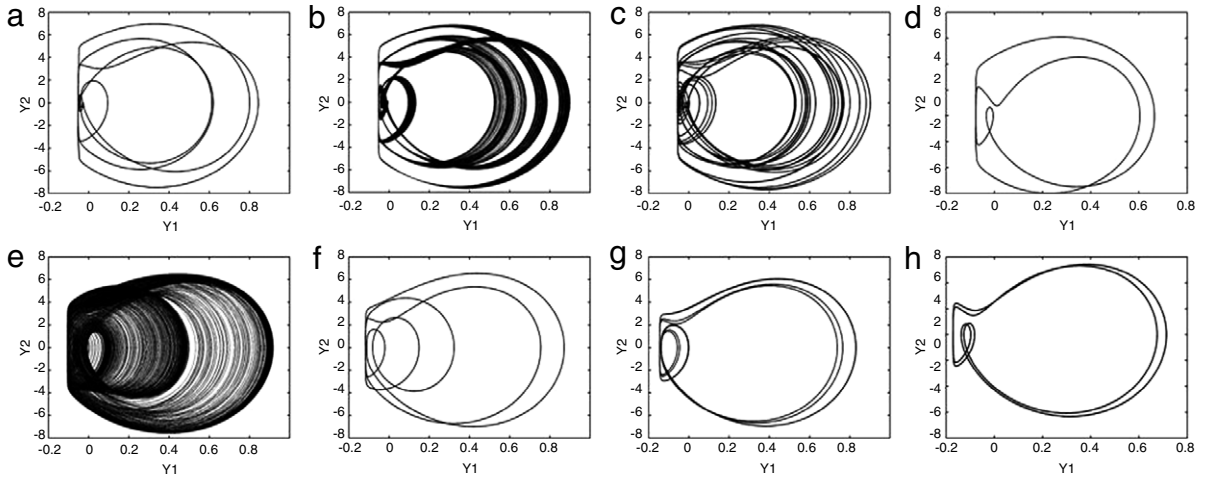

Fig. 1. Phase portraits of the probe tip displacement at vibrational amplitudes (Z) of (a) 1.10, (b) 1.12, (c) 1.19, (d) 1.58, (e) 2.19, (f) 2.40, (g) 2.97 and (h) 3.48.

3. Results and discussion

3.1. Numerical simulation results

Table 1 compares the results obtained by the DT method (DTM) and the Runge–Kutta method (RKM) for the displacement and velocity of the probe tip as a function of the vibrational amplitude of the dither piezoelectric actuator. It can be seen that for a time step of $H = 0.01$, the tip displacement and velocity values calculated by the DT method are in agreement to approximately 3–4 decimal places with those computed by the Runge–Kutta method. Moreover, at a shorter time step of $H = 0.001$, the two sets of results are in agreement to around 1–3 decimal places. Thus, the overall validity of the DT-based analytical approach is confirmed. Consequently, it can be inferred that the DT-based analytical method has a better precision than the Runge–Kutta scheme.

3.2. Phase portraits, power spectra and the maximum Lyapunov exponent

Fig. 1 presents the phase portraits of the tip displacement at various values of the vibrational amplitude, Z. In every case, the phase portrait has a non-symmetrical characteristic, i.e. the tip exhibits a nonlinear dynamic response. It is observed that the tip orbit is regular for vibrational amplitudes of $Z = 1.10$, 1.58, 2.40, 2.97 and 3.48, but irregular for $Z = 1.12$, 1.19 and 2.19. Figs. 2 and 3 present the power spectra and maximum Lyapunov exponents of the dynamic displacement for vibrational amplitudes ranging from $Z = 1.10$–3.48, respectively. The results show that at a vibrational amplitude of $Z = 1.10$, the tip performs $6T$ subharmonic motion. However, when the vibrational amplitude is increased to $Z = 1.12$, the tip response transits to one of chaotic motion proved by a positive value of the maximum Lyapunov exponent (see Fig. 3(b)). As Z is increased further to 1.19 and 1.58, the chaotic behavior is replaced by a subharmonic response. At a higher vibrational amplitude of $Z = 2.19$, the subharmonic behavior is replaced by chaotic motion once again (see Fig. 3(e)). Finally, at $Z = 2.40$, 2.97 and 3.48, the tip reverts to subharmonic motion.

3.3. Bifurcation diagrams and Poincaré maps

Fig. 4(a) and (b) plot the bifurcation diagrams of the tip displacement and tip velocity, respectively, for vibrational amplitudes ranging over $Z = 1$–5. Meanwhile, Fig. 5(a)–(h) present the Poincaré maps of the tip trajectory at $Z = 1.10$, 1.12, 1.19, 1.58, 2.19, 2.40, 2.97 and 3.48, respectively.

Fig. 4 shows that at lower values of the vibrational amplitude, i.e. $Z < 1.12$, both the displacement (Y_1) and the velocity (Y_2) of the tip exhibit a $6T$ periodic response. The existence of this $6T$ periodic motion is confirmed by the six discrete points in the Poincaré map shown in Fig. 5(a) for $Z = 1.10$. For values of the vibrational amplitude in the range $1.12 \leq Z < 1.19$, Figs. 4 and 5(b) show that the tip displacement and tip velocity exhibit a chaotic response. However, at $Z = 1.19$, the chaotic motion is replaced by multi-periodic motion (see Figs. 4 and 5(c)). Table 2 summarizes the changes in the dynamic response of the probe tip as the vibrational amplitude is increased toward a value of $Z = 5.0$. Over the range $1.19 \leq Z < 1.45$, the tip response alternates between multi-periodic and chaotic motion. At $Z = 1.58$, the multi-periodic response is replaced by $3T$ periodic motion (see Fig. 5(d)). Thereafter, Table 2 shows that chaotic behavior occurs at four different intervals of the vibrational amplitude (see Fig. 5(e), for example), while $5T$, $8T$ and $4T$ periodic motions occur at $Z = 2.40$, 2.97, 3.48, respectively (see Fig. 5(f)–(h)).

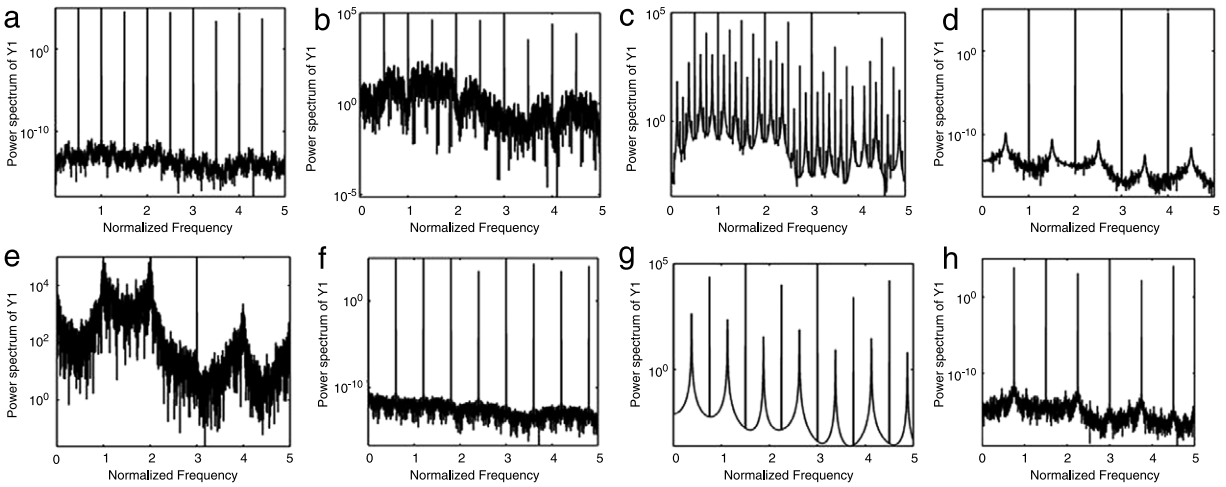

Fig. 2. Power spectra of the probe tip displacement (Y_1) at vibrational amplitudes (Z) of (a) 1.10, (b) 1.12, (c) 1.19, (d) 1.58, (e) 2.19, (f) 2.40, (g) 2.97 and (h) 3.48.

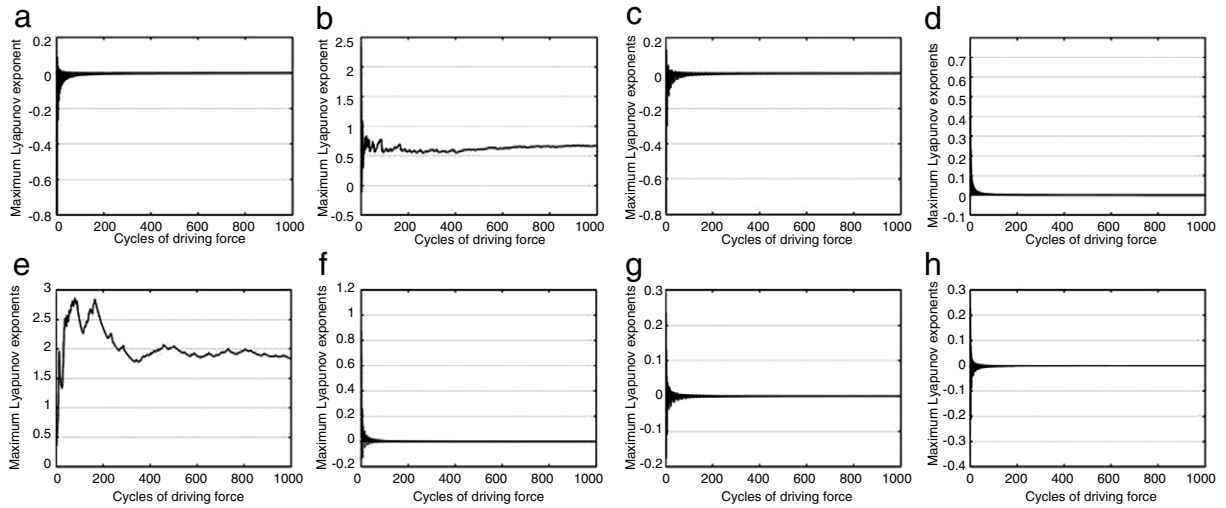

Fig. 3. Maximum Lyapunov exponents of the probe tip response at vibrational amplitudes (Z) of (a) 1.10, (b) 1.12, (c) 1.19, (d) 1.58, (e) 2.19, (f) 2.40, (g) 2.97 and (h) 3.48.

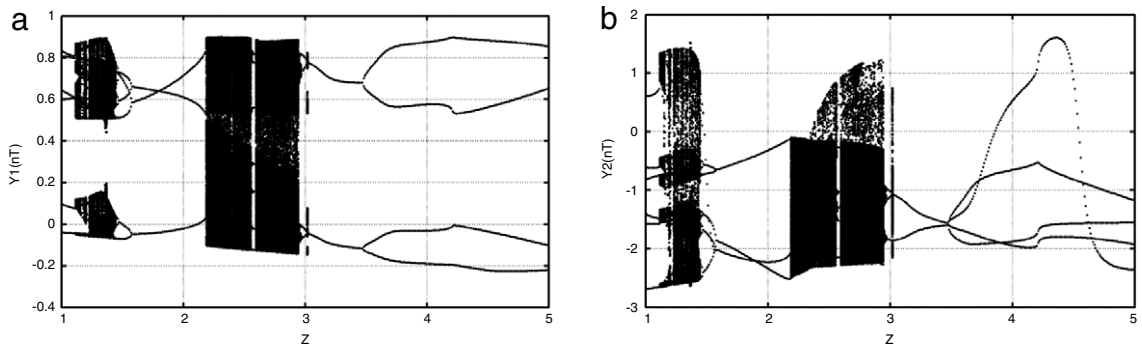

Fig. 4. Bifurcation diagrams for the probe tip displacement (a) and tip velocity (b) using vibrational amplitude (Z) as the bifurcation parameter.

Overall, the results presented in Table 2 show that depending on the value of the vibrational amplitude, the AFM probe tip may exhibit a periodic behavior, a multi-periodic behavior, or a chaotic response. It is also noted that the chaotic response

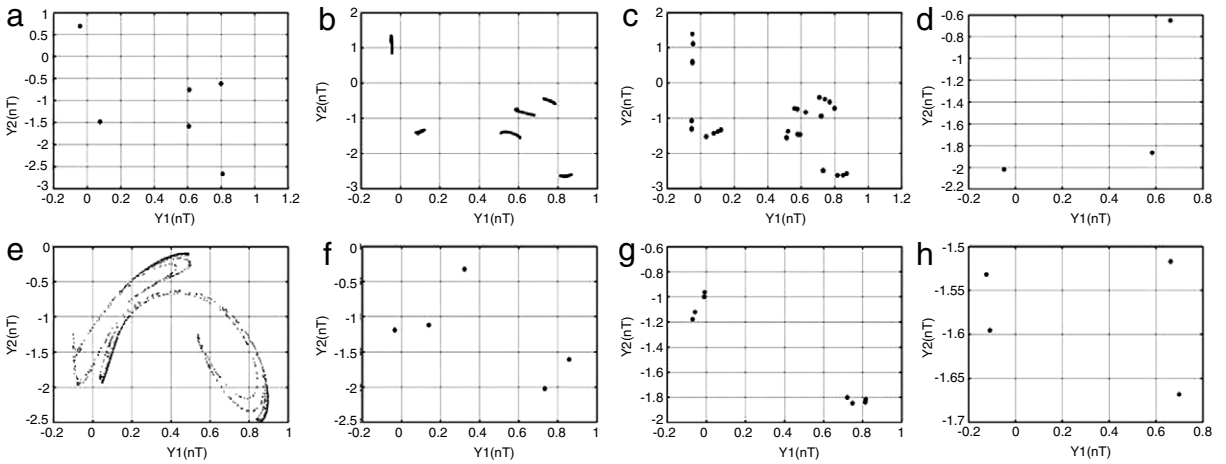

Fig. 5. Poincaré maps of the probe tip trajectory at vibrational amplitudes (Z) of (a) 1.10, (b) 1.12, (c) 1.19, (d) 1.58, (e) 2.19, (f) 2.40, (g) 2.97, and (h) 3.48.

Table 1
Comparison of results obtained by DT method (DTM) and Runge–Kutta method (RKM) for the tip displacement and tip velocity as a function of the vibrational amplitude.

Numerical method	Tip displacement Y_1 (nT)				Tip velocity Y_2 (nT)			
	$H = 0.001$		$H = 0.01$		$H = 0.001$		$H = 0.01$	
	DTM	RKM	DTM	RKM	DTM	RKM	DTM	RKM
$Z = 1.91$ ($3T$, three separated points)	−0.030921	−0.030934	−0.030945	−0.030978	−2.254711	−2.254721	−2.254701	−2.254755
	0.636085	0.636055	0.636067	0.636000	−0.413441	−0.413488	−0.413455	−0.413487
	0.681912	0.681932	0.681904	0.681989	−2.235571	−2.235556	−2.235578	−2.235576
	−0.122130	−0.122109	−0.122134	−0.122166	−1.592627	−1.592601	−1.592673	−1.592671
$Z = 3.48$ ($4T$, four separated points)	−0.141945	−0.141960	−0.141911	−0.141978	−1.537022	−1.537032	−1.537090	−1.537046
	0.6894491	0.6894431	0.6894054	0.6894451	−1.518728	−1.518744	−1.518780	−1.518719
	0.7478257	0.7478267	0.7478611	0.7478344	−1.672723	−1.672756	−1.672743	−1.672737

Table 2
Variation of the probe tip response with the vibrational amplitude over interval $1.0 \leq Z \leq 5.0$.

Z	[1.0, 1.12)	[**1.12**, **1.19**)	[1.19, 1.23)	[**1.23**, **1.28**)	[1.28, 1.29)	[**1.29**, **1.32**)
Dynamic behavior	$6T$	**Chaos**	Multi-periodic	**Chaos**	Multi-periodic	**Chaos**
Z	[1.32, 1.33)	[**1.33**, **1.35**)	[1.35, 1.36)	[**1.36**, **1.45**)	[1.45, 2.19)	[**2.19**, **2.40**)
Dynamic behavior	Multi-periodic	**Chaos**	Multi-periodic	**Chaos**	Multi-periodic, $6T$, $3T$	**Chaos**
Z	[2.40, 2.41)	[**2.41**, **2.57**)	[2.57, 2.60)	[**2.60**, **2.97**)	[2.97, 3.02)	[**3.02**, **3.03**)
Dynamic behavior	$5T$	**Chaos**	Multi-periodic	**Chaos**	$8T$, $4T$	**Chaos**
Z	[3.03, 5.0]					
Dynamic behavior	$2T$, $4T$					

always follows a subharmonic motion of the probe tip. Finally, the results presented in Fig. 1 reveal that the size of the chaotic attractor increases discontinuously as the vibrational amplitude is increased.

4. Conclusion

This study has analyzed the bifurcation characteristics of an AFM cantilever system utilizing the DT method. The validity of the proposed approach has been confirmed by comparing the results obtained for the tip displacement and tip velocity at various values of the vibrational amplitude with the solutions obtained using the Runge–Kutta method. In general, the results have shown that as the vibrational amplitude is increased from 1.0 to 5.0, the tip motion changes first from subharmonic to chaotic motion, then from chaotic to multi-periodic motion, and finally from multi-periodic motion to subharmonic motion with windows of chaotic behavior.

Acknowledgement

The financial support provided to this study by the National Science Council of the ROC under Grant Nos. NSC-98-2221-E-269-016 and NSC-99-2221-E-269-008 is greatly appreciated.

References

[1] N. Nagashima, S. Matsuoka, K. Miyahara, Nanoscopic hardness measurement by atomic force microscope, JSME Int. J. Ser. A: Mech. Mater. Eng. 39 (1996) 456–462.
[2] N.A. Burnham, A.J. Kulik, G. Germaud, G.A.D. Briggs, Nanosubharmonics: the dynamics of small nonlinear contacts, Phys. Rev. Lett. 74 (1995) 5092–5095.
[3] M. Ashhab, M. Salapaka, M. Dahleh, I. Mezic, Melnikov-based dynamical analysis of microcantilevers in scanning probe microscopy, Nonlinear Dynam. 20 (1999) 197–220.
[4] M. Ashhab, M. Salapaka, M. Dahleh, I. Mezic, Dynamical analysis and control of microcantilevers, Automatica 35 (1999) 1663–1670.
[5] A. Sebastian, M. Salapaka, D. Chen, J. Cleveland, Harmonic analysis based modeling of tapping-mode AFM, in: Proceeding of the American Control Conference, 1999, pp. 232–236.
[6] S.I. Lee, S.W. Howell, A. Raman, R. Reifenberger, Nonlinear dynamic perspectives on dynamic force microscopy, Ultramicroscopy 97 (2003) 185–198.
[7] S. Ruetzel, S.I. Lee, A. Raman, Nonlinear dynamics of atomic-force-microscope probes driven in Lennard-Jones potentials, Proc. R. Soc. Lond. Ser. A 459 (2003) 1925–1948.
[8] C.C. Wang, H.T. Yau, Application of a hybrid numerical method to the bifurcation analysis of a rigid rotor supported by a spherical gas journal bearing system, Nonlinear Dynam. 51 (2008) 515–528.